An *i*SAFT Density Functional Theory for Associating Polyatomic Molecules

Adam Bymaster and Walter G. Chapman*

Department of Chemical and Biomolecular Engineering, Rice University, 6100 South Main, Houston, Texas 77005

Received: March 24, 2010; Revised Manuscript Received: June 28, 2010

The inhomogeneous statistical associating fluid theory (*i*SAFT) is extended to associating polyatomic molecular systems, using the inhomogeneous form of the association functional. The approach provides an accurate method for modeling a wide range of complex associating polyatomic systems, capable of investigating the full range of association for any bonding scheme. Theoretical results demonstrate the ability of the theory to model problems near surfaces and in the bulk over a wide range of conditions. The examples chosen in this paper elucidate the importance of such a theory, highlighting how reversible bonding governs the structure of a fluid near a surface and in confined environments, the molecular connectivity (formation of supramolecules, star polymers, etc.), and the phase behavior of the system (including reentrant order−disorder phase transitions).

I. Introduction

Unfavorable interactions between unlike species play an important role in the phase behavior and microstructure of polymer systems, often leading to self-assembly of novel nanostructures or to undesirable macrophase separation in polymer blends. In recent years, macromolecules containing functional groups capable of forming reversible noncovalent bonds (via hydrogen bonding or ionic interactions) have attracted much attention from both experimentalists and theoreticians. The introduction of hydrogen-bonding or ionic interactions found in such associating macromolecules are important to the field of self-organizing soft materials, providing self-assembling mechanisms for a polymer blend that can potentially lead to the production of new, highly functional polymeric materials. Because of the reversible nature of such components, temperature can be used to control molecular connectivity, and hence the phase behavior (polymer−polymer miscibility, macrophase separation, and the self-assembly into mesostructures) and the unique material properties (physical properties and processability) of the system. Current and potential applications where such technology can be utilized include biosensors, separation devices, controlled drug delivery,[1] thermal manipulation of the viscosity,[2] and the development of "smart materials" with novel chemical, electrical, mechanical, and optical (light emitting) properties,[3−11] where the functionality of the material can be switched on and off via temperature controlled phase transitions.

Experimental studies have provided many insights into associating polymers (e.g., surfactants, oligomers, copolymers, and biomolecules). Given the right conditions, or the right balance between the association forces and repulsive forces between polymer segments, experiments have observed some interesting phase behaviors and material properties. For example, the design of supramacromolecules varying in size and architecture (linear, comb, star, etc.) derived from hydrogen bonding has become an area of great interest in macromolecular science, due to the interesting morphologies and physical properties present in such systems formed in the bulk.[3−14] In addition, many applications of these materials involve interactions with solid surfaces or colloidal particles and in confined geometries (adhesion, lubrication and friction, nanocomposites, blood flow and drug delivery, etc.). For this reason, a number of experiments have also investigated associating polymer solutions or melts in confined geometries and near surfaces, measuring the polymer mediated forces involved.[15−18] The aforementioned experimental studies are just a few examples of how associating/hydrogen bonding polymers can form complex molecular architectures, interesting phase transitions, and unique self-assembled patterns and microstructures. Unfortunately, although valuable, results from such studies are often confined to the specific system studied, leaving many unanswered questions.

Theoretical models will, without a doubt, play an important role in understanding and aiding the experimental design of more complex systems due to their ability to cover a wide parameter space that characterizes the polymer architectures and molecular weights, chemical incompatibilities, and bonding strengths between associating species in multicomponent polymer mixtures. One of the early theories for reversible bonding was developed by Tanaka and co-workers,[19,20] who used the random phase approximation (RPA) to study the microphase and macrophase separation transitions in systems of supramolecular diblock and comblike polymers. A shortcoming of the theory is its inability to examine the mesophase structure and stability since the free energy of the ordered microstructure is not considered (limited to investigating the stability of homogeneous phases). Later, ten Brinke and co-workers[21,22] were able to examine the mesophase structure and stability for graft and diblock copolymer systems using a higher order RPA, although the model is very laborious and restricted to the weak segregation limit. More recently, Feng et al.[23] and Lee et al.[24] have recast the field-theoretic description of supramolecular polymers to handle all segregation strengths, applying the numerical self-consistent field theory (SCFT) within this framework to investigate the self-assembly of associating supramolecular polymers. Unfortunately, mean field theories and SCFT are not accurate in describing cases of macromolecules near solid surfaces or in confined nanoslits,[25,26] where local density

* Author to whom correspondence should be addressed. Phone: (1) 713.348.4900. Fax: (1) 713 0.348.5478. E-mail: wgchap@rice.edu.

10.1021/jp102677m
Published on Web 09/08/2010

fluctuations and liquid-like ordering play a significant role. Molecular simulations have played an important role in the investigation of associating polymers for problems related both in the bulk[27−32] and in confined geometries.[33−35] However, due to the overwhelming amount of information that is retained in these computations, simulations can become computationally expensive, especially when considering supramacromolecules composed of long polymeric chains. Despite the success of all the aforementioned theoretical work, it is desirable to have a theory that is computationally efficient and capable of investigating associating polymer systems at any segregation strength and fluid density, as well as capable of providing structural and thermodynamic information not only for bulk microstructures but also for fluids near surfaces or in confined environments, which are important to many applications, as mentioned previously.

Recently, density functional theory (DFT) has emerged as a powerful theoretical tool to investigate inhomogeneous polymer systems.[36] Density functional theory is a tool with a statistical mechanics foundation that includes more physics than mean field theories and SCFT, retaining statistical segment length-level information rather than a coarse-grained representation of the polymers, at an expense significantly lower than simulation methods. Therefore, DFT can account for fluctuations in the density of the system, which is key especially near surfaces and in confined environments, where packing effects become important. As mentioned, mean-field theories and SCFT neglect fluid fluctuations and cannot retain packing effects near surfaces and in confined environments.[25,26]

Chapman[37] was the first to suggest that Wertheim's first-order thermodynamic perturbation theory (TPT1)[38−41] free energy could be used naturally within a DFT formalism for inhomogeneous associating fluids. The first DFT for associating fluids within this framework was developed by Segura et al.,[42] who described associating atomic spheres near a hydrophobic hard wall. Segura et al.[42] introduced and successfully demonstrated two approaches to include intermolecular association between atomic species. The first applies an association free energy functional based on Wertheim's TPT1 as a perturbation to a reference fluid functional, while the second approach approximates the association free energy functional using the bulk equation of state at an effective density. The second (simpler) approach has been applied with great success by numerous groups using various local or weighted density formalisms to study the structure, phase behavior, and interfacial properties of associating atomic fluids (both in confined environments and at vapor−liquid and solid−liquid interfaces).[42−48] Application of the approaches of Segura et al. for polymerization have led to the advancement of our ability to understand and investigate complex polymer systems. More recently, the second approach of Segura et al. has been applied to associating polyatomic fluids, specifically to study the structure of associating molecules at liquid−vapor interfaces,[49−52] in slit-like pores,[49] and at solid surfaces.[53] In these studies, simple association schemes were adopted on the basis of the appropriate bulk free energy expressions for a polymer segment with one association site. Such an approach, using the bulk free energy due to association, is dependent on the accuracy of the weighting functions used and, under certain conditions, does not produce the correct free energy in the limit of strong association.

In this paper, we introduce an extension to the inhomogeneous statistical associating fluid theory (*i*SAFT)[54] for associating polymer systems to remove this deficiency. The *i*SAFT density functional theory is an extension to TPT1, where the contribution to the free energy due to chain formation is derived from the inhomogeneous free energy for association for a mixture of associating spheres, taken at the complete bonding limit. The theory has already been successfully applied to study a wide range of complex polymer systems. Tripathi and Chapman[55,56] applied *i*SAFT to study polymer melts, solutions, and blends confined in slit-like pores, and Dominik et al.[57] applied the theory to real systems, calculating interfacial properties of *n*-alkanes and homopolymers. Recently, an extension of *i*SAFT was introduced by Jain et al.[54] that corrects approximations in the original theory and extends the theory to complex heteronuclear systems. For heteronuclear systems, *i*SAFT has been applied successfully to investigate block copolymers in confinement[58] and near selective surfaces,[54] tethered polymers,[59] and polymer−colloid mixtures.[60] The work in this paper for associating polymers is based on Segura et al.'s work for associating spheres, where the first approach of Segura et al. (using the inhomogeneous form of the association functional) is extended to polyatomic molecules. This approach is consistent with the *i*SAFT approach for chains, reducing exactly to the *i*SAFT chain functional in the infinite bonding limit. The resulting free energy expressions that are derived are capable of modeling complex associating systems,[61] where the full range of association can be investigated for any association scheme (for molecules having any number of association sites on any segment along a polymer chain).

In the next section, the *i*SAFT approach is presented and discussed, along with the new theoretical developments for associating chains. In section III, we demonstrate the applicability of the theory to associating polymers through various examples. The ability of the theory to handle associating polymers near surfaces and in the bulk will be demonstrated over a wide range of conditions. Further, the importance of such a theory will be elucidated through the complex behaviors observed for even the simple associating molecules chosen in this study, including the thermal reversible nature of forming larger supramolecules and molecules with complex architectures, and the resulting effect on the structure and phase behavior of the fluid (two-phase macroseparation and microphase separated lamellar morphologies, and reentrant order−disorder transitions, as observed by experiments). Finally, concluding remarks are discussed in section IV.

II. Theory

A. Model. The objective of this work is to study the full range of association for a fluid mixture composed of associating, fully flexible polymer chains. Each chain consists of m tangentially bonded spherical segments, where any number of association sites can be placed on any segment along the chain. For simplicity, in this work, all of the segments have the same diameter σ, although the theory is capable of defining each segment to be different. Here, we consider linear chains, but the theory can also be applied to associating branched chains (for the theoretical formulation for branched chains, the reader is referred to the work by Jain[62]). The polymer segments can interact through pairwise repulsive, attractive, and association contributions, given by the following pair potential

$$u(\mathbf{r}_{12}, \boldsymbol{\omega}_1, \boldsymbol{\omega}_2) = u^{\mathrm{ref}}(\mathbf{r}_{12}) + u^{\mathrm{att}}(r_{12}) + \sum_A \sum_B u_{AB}^{\mathrm{assoc}}(\mathbf{r}_{12}, \boldsymbol{\omega}_1, \boldsymbol{\omega}_2) \quad (1)$$

where u^{ref} represents the reference fluid contribution, u^{att} is the attractive contribution, u^{assoc} is the directional contribution,

$\mathbf{r}_{12}$ is the distance between segment 1 and segment 2, ω_1 and ω_2 are the orientations of the two segments, and the summations are over all association sites in the system. In this work, the reference fluid potential u^{ref} includes repulsive interactions

$$u^{\mathrm{ref}}(r_{12}) = u^{\mathrm{hs}}(r_{12}) \tag{2}$$

where the repulsive contribution between two segments on a chain is described using a hard sphere potential, given by

$$u^{\mathrm{hs}}(r_{12}) = \begin{cases} \infty, & r_{12} < \sigma \\ 0, & r_{12} \geq \sigma \end{cases} \tag{3}$$

In this work, the effective diameter is approximated as the hard-sphere diameter σ. The attractive contribution uses a cut-and-shifted Lennard-Jones (LJ) potential, with a Weeks, Chandler, and Andersen separation[63,64] at $r_{\mathrm{min}} = 2^{1/6}\sigma$.

$$u^{\mathrm{att}}(r_{12}) = \begin{cases} -\varepsilon^{\mathrm{LJ}} - u^{\mathrm{LJ}}(r_{\mathrm{cut}}), & 0 < r_{12} \leq r_{\mathrm{min}} \\ u^{\mathrm{LJ}}(r_{12}) - u^{\mathrm{LJ}}(r_{\mathrm{cut}}), & r_{\mathrm{min}} < r_{12} < r_{\mathrm{cut}} \\ 0, & r_{12} \geq r_{\mathrm{cut}} \end{cases} \tag{4}$$

where

$$u^{\mathrm{LJ}}(r_{12}) = 4\varepsilon^{\mathrm{LJ}}\left[\left(\frac{\sigma}{r_{12}}\right)^{12} - \left(\frac{\sigma}{r_{12}}\right)^{6}\right] \tag{5}$$

where $\varepsilon^{\mathrm{LJ}}$ is the molecular interaction energy and r_{cut} is the position of the potential cutoff for the LJ potential, taken to be $r_{\mathrm{cut}} = 3.5\sigma$. Any segment along a chain can have multiple association sites capable of interacting with other sites on other polymer segments. The association contribution (important to the *i*SAFT chain functional and the full range association functional) is modeled via off centered sites that interact through a square-well potential of short-range r_c. The interactions between site A on one segment and site B on another segment are modeled using the following association potential

$$u_{AB}^{\mathrm{assoc}}(\mathbf{r}_{12}, \boldsymbol{\omega}_1, \boldsymbol{\omega}_2) = \begin{cases} -\varepsilon_{AB}^{\mathrm{assoc}}, & r_{12} < r_c;\ \theta_{A1} < \theta_c;\ \theta_{B2} < \theta_c \\ 0, & \text{otherwise} \end{cases} \tag{6}$$

where θ_{A1} is the angle between the vector from the center of segment 1 to site A and the vector $\mathbf{r}_{12}$ and θ_{B2} is the angle between the vector from the center of segment 2 to site B and the vector $\mathbf{r}_{12}$. Of course, only bonding between compatible sites is permitted (two incompatible sites A and B have a bonding energy of zero, $\varepsilon_{AB}^{\mathrm{assoc}} = 0$). The radial limits of square-well association were set to $r_c = 1.05\sigma$ and the angular limit to $\theta_c = 27°$.

In addition to the pair potential between segments, an additional external field may be imposed on the system. In this work, results are presented for both bulk fluids and fluids near a hard surface. The external field introduced into the system by the hard wall is given by

$$V^{\mathrm{ext}}(z) = \begin{cases} \infty, & z < \dfrac{\sigma}{2} \\ 0, & \text{otherwise} \end{cases} \tag{7}$$

where z is the distance normal to the surface.

B. iSAFT Density Functional Theory. The density functional theory is formulated in the grand canonical ensemble, which has a fixed volume (V), temperature (T), and chemical potential (μ). The starting point of the density functional theory is the development of an expression for the grand potential, Ω, as a functional of the equilibrium polymer density profile $\rho(r)$. From this, the desired thermodynamic and structural properties of the system can be determined. In this work, we consider associating fluid mixtures composed of polymeric components (C_1, C_2, ... , C_n). The grand potential can be related to the Helmholtz free energy functional $A[\rho(r)]$ through the Legendre transform[65]

$$\Omega[\rho_i^{(C1)}(\mathbf{r}), \rho_i^{(C2)}(\mathbf{r}), ...] = A[\rho_i^{(C1)}(\mathbf{r}), \rho_i^{(C2)}(\mathbf{r}), ...] - \sum_{l=C1,C2...} \sum_{i=1}^{m_l} \int \mathrm{d}\mathbf{r}' \rho_i^{(l)}(\mathbf{r}')(\mu_{i,l} - V_{\mathrm{ext}}^{i,l}(\mathbf{r}')) \tag{8}$$

where $\rho_i^{(l)}(r)$ is the density of the ith segment on chain l at position $\mathbf{r}$, m_l is the chain length of chain l, $\mu_{i,l}$ is the bulk chemical potential of that segment, and $V_{\mathrm{ext}}^{i,l}$ is the external field acting on that segment. The first summation is over all chains l in the mixture (C_1, C_2, ... , C_n), and the second summation is over all segments on chain l. Since *i*SAFT is a segment-based DFT that treats each segment differently, we can simplify this notation by combining these two sums to an equivalent sum over all segments (N) in the system, where $N = m_{C1} + m_{C2} + ... m_{Cn}$. At equilibrium, the following condition is satisfied

$$\frac{\delta\Omega}{\delta\rho_i(\mathbf{r})} = 0 \qquad \forall i = 1, N \tag{9}$$

Solving this set of Euler−Lagrange equations gives the equilibrium density profile of the segments. The total Helmholtz free energy functional can be decomposed into an ideal and excess contribution

$$A[\rho_i(\mathbf{r})] = A^{\mathrm{id}}[\rho_i(\mathbf{r})] + A^{\mathrm{ex,hs}}[\rho_i(\mathbf{r})] + A^{\mathrm{ex,chain}}[\rho_i(\mathbf{r})] + A^{\mathrm{ex,att}}[\rho_i(\mathbf{r})] + A^{\mathrm{ex,assoc}}[\rho_i(\mathbf{r})] \tag{10}$$

where the excess contribution consists of changes in the free energy due to excluded volume (hs), chain connectivity (chain), long-range attraction (att), and association (assoc), over the ideal gas (id) state of the atomic mixture.

B.1. Free Energy Functionals. The ideal free energy functional is known exactly from statistical mechanics

$$\beta A^{\mathrm{id}}[\rho_i(\mathbf{r})] = \int \mathrm{d}\mathbf{r}_1 \sum_{i=1}^{N} \rho_i(\mathbf{r}_1)[\ln \rho_i(\mathbf{r}_1) - 1] \tag{11}$$

where the temperature-dependent term (the de Broglie wavelength Λ) has been dropped, since it is not density dependent and hence does not affect the structure or thermodynamics of the fluid. The inverse temperature is represented by $\beta = 1/k_bT$,

where k_b is Boltzmann's constant. The free energy due to excluded volume/short-range repulsion, $A^{ex,hs}$, is calculated using Rosenfeld's fundamental measure theory (FMT),[66,67] postulated to have the form

$$\beta A^{ex,hs}[\rho_i(\mathbf{r})] = \int d\mathbf{r}\Phi^{ex,hs}[n_\alpha(\mathbf{r})] \tag{12}$$

where $\Phi^{ex,hs}[n_\alpha(\mathbf{r})]$ is the excess Helmholtz free energy density due to the hard core interactions. $\Phi^{ex,hs}[n_\alpha(\mathbf{r})]$ is assumed to be a function of only the system averaged fundamental geometric measures, $n_\alpha(\mathbf{r})$, of the particles, given by

$$n_\alpha(\mathbf{r}) = \sum_{l=C1,C2,...} \sum_{i=1}^{m_l} n_{\alpha,i}(\mathbf{r}) = \sum_{i=1}^{N} \int \rho_i(\mathbf{r}_1) w_i^{(\alpha)}(\mathbf{r} - \mathbf{r}_1)\, d\mathbf{r}_1 \tag{13}$$

where $\alpha = 0$, 1, 2, 3, $V1$, and $V2$ are representative of the six scalar and vector weight functions used in Rosenfeld's formalism.[66,67] In the FMT formalism, $\Phi^{ex,hs}[n_\alpha(\mathbf{r})]$ has the form

$$\Phi^{ex,hs}[n_\alpha(\mathbf{r})] = -n_0 \ln(1 - n_3) + \frac{n_1 n_2 - \mathbf{n}_{v1}\cdot\mathbf{n}_{v2}}{1 - n_3} + \frac{{n_2}^3 - 3n_2\mathbf{n}_{v2}\cdot\mathbf{n}_{v2}}{24\pi(1 - n_3)^2} \tag{14}$$

The free energy due to long-range attraction can be included within the mean field approximation[68]

$$A^{ex,att}[\rho_i(\mathbf{r})] = \frac{1}{2}\sum_{i=1}^{N}\sum_{j=1}^{N} \int d\mathbf{r}_1\, d\mathbf{r}_2\, u_{ij}^{att}(|\mathbf{r}_2 - \mathbf{r}_1|)\rho_i(\mathbf{r}_1)\rho_i(\mathbf{r}_2) \tag{15}$$

Since the focus of this work is to present an accurate free energy functional for association, we consider the above formulation to be sufficient for this study. This formulation of the dispersion term has been demonstrated to perform well in comparison to simulation data. Techniques to improve the long-range attraction term described in the literature include adopting non-mean-field prescriptions using the first-order mean spherical approximation developed by Tang and Wu,[69] or using a weighted density approximation developed by Muller et al.[70] and demonstrated by Reddy and Yethiraj.[71]

The association functional was originally developed by Chapman[37,42] by extending TPT1. Below, the association functional is given for an associating polyatomic mixture

$$\beta A^{ex,assoc}[\rho_i(\mathbf{r})] = \int d\mathbf{r}_1 \sum_{i=1}^{N} \rho_i(\mathbf{r}_1) \times \sum_{A\in\Gamma^{(i)}} \left(\ln \chi_A^i(\mathbf{r}_1) - \frac{\chi_A^i(\mathbf{r}_1)}{2} + \frac{1}{2}\right) \tag{16}$$

The first summation is over all segments (on all chains in the mixture), and the second summation is over all of the associating sites on segment i of chain l. $\chi_A^i(\mathbf{r}_1)$ represents the fraction of segments of type i which are not bonded at their site A. This unbonded fraction is given by

$$\chi_A^i(\mathbf{r}_1) = \frac{1}{1 + \int d\mathbf{r}_2 \sum_{k=1}^{N} \rho_k(\mathbf{r}_2) \sum_{B\in\Gamma^{(k)}} \chi_B^k(\mathbf{r}_2)\Delta_{AB}^{ik}(\mathbf{r}_1, \mathbf{r}_2)} \tag{17}$$

The degree of association is controlled by the term

$$\Delta_{AB}^{ik}(\mathbf{r}_1, \mathbf{r}_2) = \kappa[\exp(\beta\varepsilon_{Ai,Bk}^{assoc}) - 1]y^{ik}(\mathbf{r}_1, \mathbf{r}_2) \tag{18}$$

Here, κ represents a geometric constant (accounts for the entropic cost associated with the orientations and bond volume of the associating segments), $\varepsilon_{Ai,Bk}^{assoc}$ is the associating energy between compatible sites A and B on segments i and k, and $y^{ik}(\mathbf{r}_1,\mathbf{r}_2)$ is the cavity correlation function for the inhomogeneous hard sphere reference fluid. In this work, we make a geometric mean approximation for the distribution function, similar in spirit to the work of Toxvaerd[72] and in the derivation of the chain term in *i*SAFT.[54] We approximate the inhomogeneous potential of mean force as the average of the potential of mean force at the two segment positions. Although not stated, this approximation is implicit in other DFTs based on TPT1. The cavity correlation function is approximated using its bulk value[73] evaluated at contact using a weighted density[55,56]

$$y^{ik}(r_{12}, \mathbf{r}_1, \mathbf{r}_2) \approx [y^{ik}(\sigma, \bar{\zeta}(\mathbf{r}_1)) \times y^{ik}(\sigma, \bar{\zeta}(\mathbf{r}_2))]^{1/2} \tag{19}$$

where $\overline{\zeta_\alpha}(\mathbf{r}_1) = (\pi/6)\sum_{j=1}^{N} \bar{\rho}_j(\mathbf{r}_1)\sigma^\alpha$ ($\alpha = 0$, 1, 2, 3) and $\bar{\rho}_j(\mathbf{r}_1)$ represents the weighted density of segment j at position $\mathbf{r}_1$. In this work, the simple weighting is used

$$\bar{\rho}_j(\mathbf{r}_1) = \frac{3}{4\pi\sigma^3}\int_{|\mathbf{r}_1-\mathbf{r}_2|<\sigma} d\mathbf{r}_2\, \rho_j(\mathbf{r}_2) \tag{20}$$

It has already been demonstrated how the association free energy functional based on Wertheim's first-order thermodynamic perturbation theory can be used in the limit of complete association to form a polyatomic fluid (tangentially bonded chains) from a mixture of associating spheres.[54,59,60] In this paper, we demonstrate how, starting from the same form of the inhomogeneous association free energy functional, the full range of association can be investigated. When deriving the chain contribution to the free energy, $\varepsilon^{assoc} \to \infty$ and an additional bonding potential $\nu_{bond}^{ik}(\mathbf{r}_1,\mathbf{r}_2)$ for tangentially bonded segments is included in the above expression[54−57,59,60] (see the Supporting Information for details).

B.2. Free Energy Functional Derivatives. All of the functional derivatives are essential in solving the Euler−Lagrange equations (from eq 9), which give the density profile. The functional derivative of the free energies is given by

$$\frac{\delta\beta A^{id}}{\delta\rho_j(\mathbf{r})} = \ln \rho_j(\mathbf{r}) \tag{21}$$

$$\frac{\delta\beta A^{\text{ex,hs}}}{\delta\rho_j(\mathbf{r})} = \int d\mathbf{r}_1 \frac{\delta\Phi^{\text{ex,hs}}[n_i(\mathbf{r}_1)]}{\delta\rho_j(\mathbf{r})} \quad (22)$$

$$\frac{\delta\beta A^{\text{ex,att}}}{\delta\rho_j(\mathbf{r})} = \sum_{i=1}^{N} \int d\mathbf{r}_1 \beta u_{ij}^{\text{att}}(|\mathbf{r} - \mathbf{r}_1|)\rho_i(\mathbf{r}_1) \quad (23)$$

$$\frac{\delta\beta A^{\text{ex,chain}}}{\delta\rho_j(\mathbf{r})} = \sum_{A\in\Gamma^{(j)}} \ln \chi_A^j(\mathbf{r}) - \frac{1}{2}\sum_{k=1}^{N}\sum_{k'}^{\{k'\}} \int \rho_k(\mathbf{r}_1)\frac{\delta \ln y^{kk'}(\bar{\zeta}(\mathbf{r}_1))}{\delta\rho_j(\mathbf{r})} d\mathbf{r}_1 \quad (24)$$

In the above chain functional derivative, all association sites considered in this expression are representative of the sites responsible for the molecular connectivity of the chains in the mixture, which are formed by applying the limit of complete association ($\{k'\}$ is the set of all segments bonded to segment k on chain l). Details regarding the above functional derivatives are given in earlier works.[54,59,60] Below, the functional derivative for the full range of association is given.[61] Details of this derivation can be found in the Supporting Information.

$$\frac{\delta\beta A^{\text{ex,assoc}}}{\delta\rho_j(\mathbf{r})} = \sum_{A\in\Gamma^{(j)}} (\ln \chi_A^j(\mathbf{r})) - \frac{1}{2}\sum_{i=1}^{N}\sum_{k=1}^{N} \int d\mathbf{r}_1 \rho_i(\mathbf{r}_1) \times \sum_{A\in\Gamma^{(i)}} (1 - \chi_A^i(\mathbf{r}_1))\left[\frac{\delta \ln y^{ik}(\bar{\zeta}(\mathbf{r}_1))}{\delta\rho_j(\mathbf{r})}\right] \quad (25)$$

The above expression is the final form for associating chains. The term $[\delta \ln y^{ik}(\bar{\zeta}(\mathbf{r}_1))]/\delta\rho_j(\mathbf{r})$ only contributes for segments k with association sites that are eligible to bond to sites located on segment i. Substituting the functional derivatives of the free energies in the Euler−Lagrange (eq 9) allows for the solution of the equilibrium density profile of the polymer segments. The reader is referred to the Supporting Information and previous work[54,59,60] for details regarding the expressions for the density profile and equilibrium grand free energy.

III. Results and Discussion

The primary focus of this section is to establish the capability of the theory to handle a wide range of associating polymer systems. In this section, results are presented for associating mixtures near surfaces and in the bulk, over a wide range of conditions in comparison with available simulation and experimental data. The associating schemes and mixtures investigated in this work are illustrated in Figure 1. First, the theory is validated near a hard wall, illustrating the effect of varying the association strength on the behavior of the fluid (neglecting dispersion interactions). Next, an associating mixture is considered at high association strengths, showing how different association schemes can result in complex molecular architectures or supramolecules (see Figure 1b). These results are compared and agree very well with available simulation results for a star polymer confined between two hard surfaces from Yethiraj and Hall.[74] Finally, the theory is demonstrated for a challenging problem of interest, a bulk associating mixture of two homopolymers with end functional segments capable of reversibly bonding to form supramolecular diblock copolymers. For this system, we systematically explore the phase diagram, demonstrating how competing effects (chain length, chemical incompatibilities, and bonding energies) can result in unique polymer morphologies (microphase lamellar separation, two-phase macrophase separation) and complex phase behavior (regions of reentrant order−disorder transitions in the phase diagram, as observed in experiments). These examples elucidate the ability of the theory to correctly model and capture the complex fluid behavior for associating polymer systems. Such a theory is important to the understanding and development in many problems and applications (discussed in the Introduction) where temperature can be used to control the reversible bonding, phase behavior, and material properties of the system.

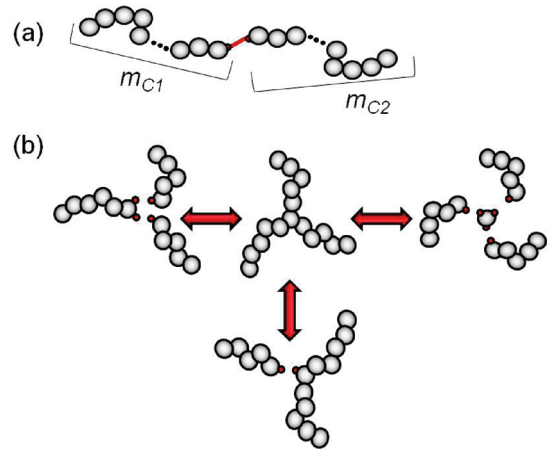

Figure 1. Illustration of associating schemes used in this work: (a) end associating functional groups (terminal associating segment with one site) on a homopolymer of any arbitrary length (as indicated by "•••" in figure); (b) schemes capable of forming a star polymer architecture (3 arms, $N = 16$) at high association strengths. In the figure, m_l represents the chain length of polymeric component l ($l = C_1, C_2, \ldots, C_n$) and N represents all segments in the system $N = m_{C1} + m_{C2} + \ldots m_{Cn}$.

A. Associating Polymers near a Wall. First, we apply the proposed theory to a simple model of associating molecules and investigate the structure of the fluid near a hard surface. As discussed previously in section I, there are two approaches to include association.[42] The inhomogeneous approach (the proposed approach, outlined in section II) and the weighted approach (included below) are compared in Figure 2. The weighted approach approximates the association free energy functional using the bulk equation of state evaluated at a weighted density

$$\beta A^{\text{ex,assoc}}[\rho_i(\mathbf{r})] = \int d\mathbf{r}_1 \sum_{i=1}^{N} \rho_i(\mathbf{r}_1) \times \sum_{A\in\Gamma^{(i)}} \left(\ln \bar{\chi}_A^i(\mathbf{r}_1) - \frac{\bar{\chi}_A^i(\mathbf{r}_1)}{2} + \frac{1}{2}\right) \quad (26)$$

where the fraction of segments of type i which are not bonded at their site A is given by

$$\bar{\chi}_A^i(\mathbf{r}_1) = \frac{1}{1 + \sum_{k=1}^{N} \bar{\rho}_k(\mathbf{r}_1) \sum_{B\in\Gamma^{(k)}} \bar{\chi}_B^k(\mathbf{r}_1)\Delta_{AB}^{ik}(\mathbf{r}_1)} \quad (27)$$

and $\Delta_{AB}^{ik}(\mathbf{r}_1)$ is defined as before in eq 18. The accuracy of the weighted approach is dependent on the weight functions used. For comparison, the same weighted density used in the calculation of

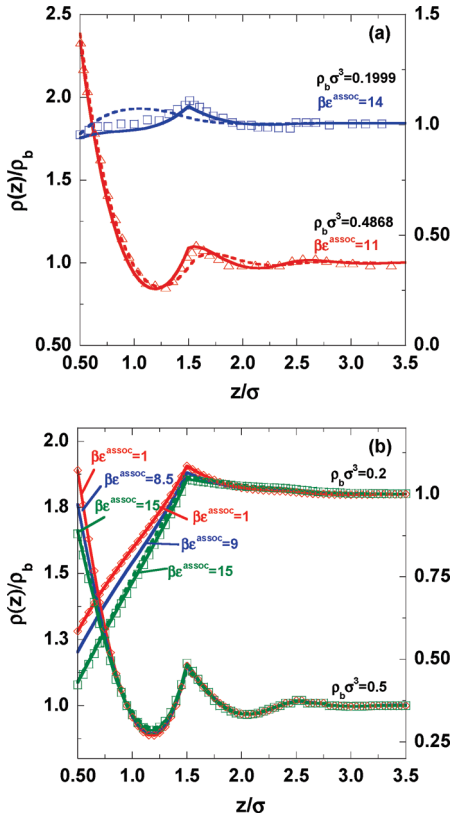

Figure 2. Effect of varying bonding strength (ε^{assoc}) on the structure of an associating fluid near a smooth hard surface. Here, dispersion interactions are neglected, $\varepsilon^{LJ} = 0$. Lines represent theoretical results using the inhomogeneous association free energy functional (solid lines) and the weighted bulk form association free energy functional (dashed lines, provided for comparison at highest association energies). In part a, a dimerizing hard sphere fluid (scheme from Figure 1a, $m = 1$) is presented at $\rho_b\sigma^3 = 0.1999$ and $\beta\varepsilon^{assoc} = 14$ (right vertical axis) and at $\rho_b\sigma^3 = 0.4868$ and $\beta\varepsilon^{assoc} = 11$ (left vertical axis). Symbols represent simulation data.[45] In part b, the structure of an associating polymer fluid (scheme from Figure 1a, $m = 4$) is presented at $\rho_b\sigma^3 = 0.2$ (right vertical axis) and $\rho_b\sigma^3 = 0.5$ (left vertical axis). Here, the symbols represent results for a nonassociating 4mer (red ◊) and 8mer (green □).

the cavity correlation function in eqs 19 and 20 is used in the second approach. The functional derivative can be found in previous work.[46]

Figure 2 captures the effect of varying the association strength on the structure of a pure associating fluid near a hard wall. Depletion from the surface is captured at low concentrations, while packing effects increase the accumulation of segments at the surface at higher densities (dispersion interactions are neglected here, $\varepsilon^{LJ} = 0$). First, in Figure 2a, the simple case of a dimerizing hard sphere fluid (associating scheme from Figure 1a with $m = 1$) is presented at $\rho_b\sigma^3 = 0.1999$ and $\varepsilon^{assoc}/k_bT = 14$ (right vertical axis) and at $\rho_b\sigma^3 = 0.4868$ and $\varepsilon^{assoc}/k_bT = 11$ (left vertical axis), in comparison with simulation data.[45] From these results, it is clear that, at lower densities and high association energies, the weighted approach is unable to capture the correct structure of the fluid even qualitatively (these results are consistent with the results found previously by Segura et al.[45] using the Tarazona[75,76] weight functions). In contrast, the inhomogeneous form provides a more accurate expression for the free energy of association and is able to capture the correct structure of the fluid at these conditions. At higher densities, the weighted approach is much improved; however, the inhomogeneous approach is still superior and in better quantitative agreement with the simulations. In Figure 2b, the model assumes a pure homopolymer ($m = 4$) where a single association site is located on one of the terminal segments of the chain and is able to bond with other chains in the fluid (see the association scheme presented in Figure 1a). In Figure 2b, the symbols represent *i*SAFT results for a nonassociating 4mer (red ◊) and 8mer (green □), while the lines represent *i*SAFT results for the associating 4mers. The weighted approach is included for comparison at the highest association strengths (dashed lines are barely visible). In Figure 2b, the results indicate that both approaches capture the correct behavior at high and low densities for associating chains, though there are some minor quantitative differences (hard to distinguish in figure). Such results suggest that the weighted approach may be sensitive to the concentration of associating segments in the system. In this example, as the chain length increases, the effect of association decreases and the concentration of bonding segments in the fluid decreases, scaling as $1/m$. In comparing parts a and b of Figure 2, both approaches are accurate for lower concentrations of associating segments (Figure 2b), but the weighted approach produces less accurate structures under certain conditions (high association strengths at lower densities) for systems with a higher concentration of associating segments (Figure 2a). The inhomogeneous approach developed here has the advantage that, in the strong association limit, the model predicts the exact ideal chain free energy functional and segment distribution, an advantage over other density functional theories that constrain bond connectivity through the ideal chain functional. Differences between the approaches will be most obvious at low density with strong association at multiple sites. All remaining results presented are therefore based on the inhomogeneous form of the association functional, because of its versatility and ability to handle any association scheme, especially for more complex heteronuclear systems that may involve many associating segments. From Figure 2b, as expected, the behavior of an associating linear chain (with one associating site on a terminal segment) varies between that of a nonassociating chain of the same length (in this case of a 4mer) and that for a nonassociating chain twice as large (8mer). When the association energy is low ($\varepsilon^{assoc}/k_bT = 1$), the profiles are similar to the nonassociating 4mer. As the association energy increases, the concentration of 8mers in the mixture also increases and approaches the behavior of a pure nonassociating 8mer. Higher association energies result in higher concentrations of longer chains, which lead to lower contact densities at the surface due to conformational entropic effects.

Of course, more involved association schemes, where the polymer molecule may involve multiple associating segments and/or multiple sites, can lead to more complex polymer architectures (at high association strengths). Figure 3 demonstrates such an example, again considering only association interactions. Here, we consider a polymer mixture using any of the schemes presented in Figure 1b. High bonding strengths (results in Figure 3 use $\varepsilon^{assoc}/k_bT \geq 30$) create a large population of star polymers (3 arms, $N = 16$) in the melt, so that we are able to compare the structure of the fluid confined between two hard surfaces (separated at distance $H = 16\sigma$) with available simulation data by Yethiraj and Hall.[74] The agreement between the theory and the simulation results is good, capturing the competition between packing and entropic effects at different average packing fractions (η_{avg}) of the fluid in the confined space. Symbols represent simulation data, while solid lines represent *i*SAFT results. In the figure, the density profiles are normalized to their bulk value (ρ_b). Because the profiles are

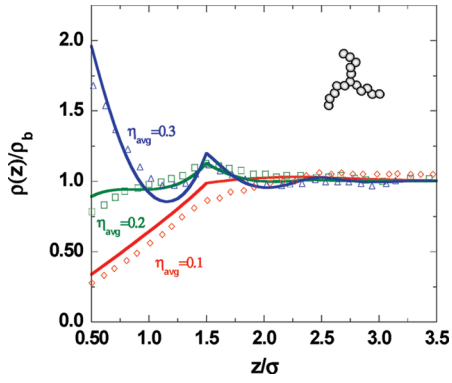

Figure 3. Density distribution of a star polymer (3 arms, $N = 16$) between two hard walls separated at a distance of $H = 16\sigma$ (profile only given near one wall) at $\eta_{avg} = 0.3$, 0.2, and 0.1. A high population of star polymers is formed in the melt at high bonding strengths (e.g., $\beta\varepsilon^{assoc} = 30$) using any of the association schemes given in Figure 1b. Symbols represent simulation data from Yethiraj and Hall,[74] and lines represent results from *i*SAFT. The density profiles are normalized to the bulk value.

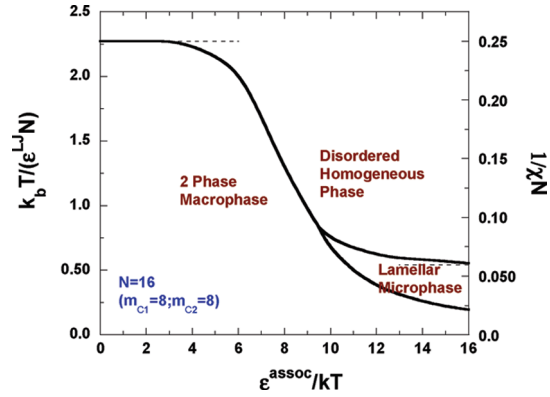

Figure 4. Phase diagram for an associating polymer mixture. The binary mixture is at a total segment density of $\rho_b\sigma^3 = 0.85$ and is symmetric ($m_{C1} = 8$ and $m_{C2} = 8$, equal concentrations, association scheme from Figure 1a). Three distinct phases are present in the phase diagram: a homogeneous disordered phase, a two-phase macrophase, and a lamellar microphase.

symmetric about the middle of the confinement, only the profiles near one of the surfaces are shown. The results presented in Figure 3 (in the limit of strong association) are consistent with the results previously published by Malijevsky et al.[77] for star polymers. Malijevsky et al. generalized the free energy contribution due to the formation of chains with arms (star and branched chains) using a similar approach to Yu and Wu,[78] who assume that chain connectivity can be formulated on the basis of a bulk equation of state. In our model, the concentration of star polymer formed in the melt, and thus the fluid structure at the surface, can be controlled by the temperature (or varying reversible bonding energy). Differences in the contact density can be attributed to inaccuracies in the bulk equation of state (which overpredicts the pressure). As Malijevsky et al.[77] demonstrated, the densities within the region adjacent to the wall can be improved slightly by using the TPT2 contribution to the free energy. Even more complex association schemes can be applied to multicomponent mixtures to form star and comb polymers with arms of arbitrary lengths.

In this section, the ability of the *i*SAFT DFT to capture compressibility effects and the local structure of associating macromolecules near surfaces and in confined environments was demonstrated. Future studies using *i*SAFT could provide interesting insights into some of today's more challenging problems involving associating polymers near surfaces and in confined environments, including lubrication and friction, adhesion, nanocomposites, blood flow, and drug delivery.

B. Self-Assembly of Associating Polymers into Inhomogeneous Phases. In this section, we consider a binary mixture of two homopolymers of equal concentrations and chain lengths. Homopolymer C_1 is assigned one association site (site A) on a terminal bead (see association scheme in Figure 1a) that is allowed to reversibly bond to a similar site (site B) on the other component in the mixture (C_2). All systems considered in this section have a melt-like, total segment density of $\rho_b\sigma^3 = 0.85$. In this model, the dispersion energy defines the chemical incompatibilities of the two components in the mixture, where $\varepsilon^{C1,C1} = \varepsilon^{C2,C2} = \varepsilon^{LJ}$ and $\varepsilon^{C1,C2} = 0$. This parameter can be correlated with the traditional Flory−Huggins interaction parameter χ (see Figure 4).[58,79] This particular system is of high interest because of the broad range of phase behaviors possible when unlike polymer species are linked by reversible bonds into supramolecular polymers, in this case supramolecular diblock copolymers. It is well-known from experiments[9,80] that reentrant behavior occurs for low molecular weight associating polymers upon raising or lowering the temperature. Here, we systematically explore the phase diagram by varying the chain length ($N = m_{C1} + m_{C2}$), the dispersion energy (ε^{LJ}), and the association bonding energy (ε_{AB}^{assoc}), covering all segregation regimes.

Figure 4 demonstrates how competing effects between the association bonding energy and the dispersion energy can lead to three distinct phases: a homogeneous disordered phase (where C_1 and C_2 are miscible), a macrophase separation (liquid−liquid immiscibility), and a microphase lamellar separation. From the figure, low dispersion energies (low degree of incompatibility between the two components) and low association energies lead to a homogeneous disordered phase (DIS). Upon increasing ε^{LJ} at low association energies, a phase transition from the disordered state to a macrophase separation (2 phase) occurs. This occurs due to the increased incompatibility between the two components in the mixture and the low concentration of copolymer present in the system. Note that increasing ε^{LJ} at fixed ε^{assoc} does not correspond to decreasing temperature, since ε^{assoc} is also temperature dependent (addressed below). An example of macrophase separation is illustrated in Figure 5a, characterized by the C_1 and C_2 rich phases. However, as the association strength is increased, the concentration of diblock copolymer increases, thus increasing the probability of microphase separation (see Figure 4). Figure 5b illustrates a typical microphase structure, where the increased concentration of diblock copolymers ($N = 16$) may self-assemble into a lamellar phase.

When both the dispersion energy and the association energy are high, macrophase or microphase separation can occur. The phase boundary between these two phases can be determined by comparing the free energies to establish the more stable phase (the more thermodynamically favorable phase). In comparing the free energies between the macrophase and microphase, first the equilibrium lamellar period (L_e) for the microphase must be determined (as changing the bonding energy or the dispersion energy affects the equilibrium spacing of the lamellar structure). This is done by calculating the grand potential (Ω) of the system. Figure 6 plots the grand free energy per volume for different association and dispersion strengths, as a function of the width of the computational domain. Similar results and trends are predicted under other sets of conditions. From the figure, the

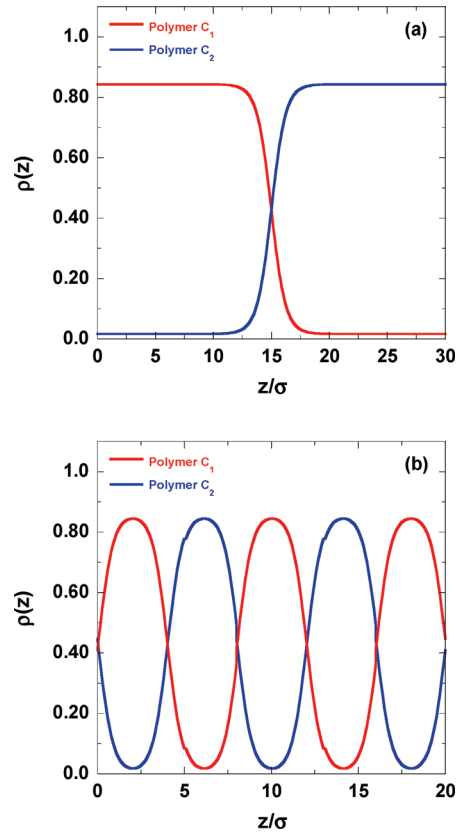

Figure 5. (a) Example of a typical density profile for a liquid−liquid macrophase separation. (b) Example of a typical density profile for a lamellar microphase separation. A lamellar phase can form at higher association strengths where a higher concentration of copolymer exists in the mixture. The lamellar period for this example structure is $L = 8\sigma$. The equilibrium lamellar period (L_e) for the microphase is determined via the grand potential (see Figure 6; changing the bonding energy or the dispersion energy affects the equilibrium spacing of the lamellar structure).

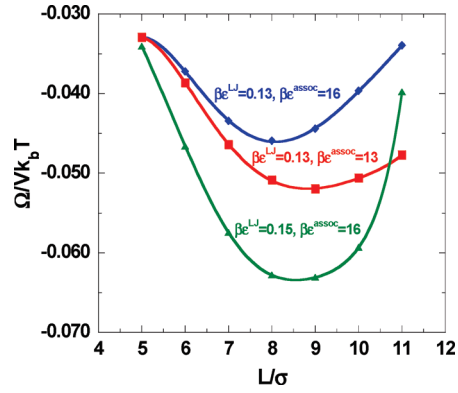

Figure 6. Grand free energy per volume as a function of the computational domain at given association and dispersion energies ($m_{C1} = 8$, $m_{C2} = 8$, $N = 16$). The equilibrium spacing is determined as the width at which a minimum in the free energy occurs. Similar results and trends are predicted under other sets of conditions and chain lengths.

equilibrium spacing is determined as the width at which a minimum in the free energy occurs. For the lamellar phases, at a given association energy, the equilibrium lamellar period increases and the equilibrium free energy decreases as the dispersion energy becomes larger (the increasing incompatibility between the two components promotes a decreasing number of interfaces to minimize the number of contacts between C_1 and C_2). At fixed dispersion energy, decreasing the association energy results in a larger L_e (and decreases the equilibrium free energy). Both trends encourage macrophase separation, as the lamellar phase transitions into a liquid−liquid phase as reflected in the phase diagram in Figure 4.

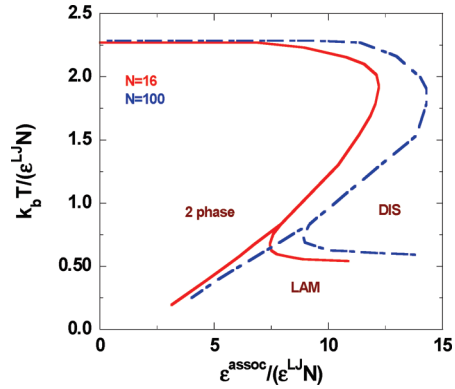

Figure 7. Phase diagram for associating polymer mixtures ($N = 16$ and $N = 100$) highlighting the effect of chain length and temperature on the phase behavior. Three distinct phases are present in the phase diagram: a homogeneous disordered phase (DIS), a macrophase (2 phase), and a lamellar microphase (LAM). Reentrant behavior is observed (DIS−2 phase−DIS and LAM−DIS−LAM) upon raising/lowering the temperature.

While Figure 4 highlights important features of the phase diagram, it does not show a clear dependence on temperature (as both coordinates are temperature dependent). Figure 7 provides the phase diagram after scaling the thermal energy (k_bT) and the bonding energy (ε^{assoc}) by the total dispersion interaction energy of the diblock chain ($\varepsilon^{LJ}N$). This provides a dimensionless temperature versus dimensionless bonding energy to demonstrate the effect of changing the temperature at a fixed ratio of ($\varepsilon^{assoc}/\varepsilon^{LJ}N$). When looking at this phase diagram, one notices regions where reentrant behavior occurs. First, for $N = 16$, it is obvious that reentrant behavior occurs upon raising/lowering the temperature over a large band of higher energy ratios ($\varepsilon^{assoc}/\varepsilon^{LJ}N \approx 7.90-12.25$), predicting a sequence of transitions from disordered to macrophase to disordered phases. Here, such reentrant behavior is due to hydrogen-bonding interactions (similar behavior drives closed loop LL immiscibility, which is unique to unlike, associating mixtures). At low temperatures, the unlike pairs permit association and complete mixing (association between unlike species in the mixture results in the low temperature miscibility of the system, as indicated by the low temperature DIS). As the temperature is increased, many of these association bonds are broken, leading to immiscibility (two-phase separation). Increasing the temperature further leads to increased kinetic motion in the fluid, which results in increased miscibility and complete mixing (high temperature DIS). A more narrow band ($\varepsilon^{assoc}/\varepsilon^{LJ}N \approx 7.45-7.9$) displays transitions from lamellar to disordered to lamellar phases upon raising and lowering the temperature. Similar bands of reentrant behavior are also predicted in Figure 7 for longer diblock chains ($N = 100$). Homogeneous reentrant behavior has been observed experimentally.[9,80] To our knowledge, no experiments have demonstrated reentrant behavior of an inhomogeneous phase in a supramolecular polymer system, although recent theoretical results (SCFT) by Feng et al.[23] do predict inhomogeneous reentrant behavior involving a lamellar phase, consistent with the results presented here (it is not surprising to also see SCFT capture this unique phase behavior for this bulk system). As expected, there are some quantitative differences between the results of this work and the work of Feng et al. It will therefore be interesting to see if such reentrant

inhomogeneous behavior can be observed in future experiments, based on the results of both theories. Finally, Figure 7 also highlights the effect of increasing the chain length in the associating mixture. As the chain length increases, the concentration of bonding segments in the mixture decreases (scales as $1/N$). As a result, for increasing N, a higher bonding energy is required to increase the concentration of copolymer in the mixture (needed to encourage microphase separation and a homogeneous disordered phase) and thus the two-phase region becomes larger.

The *i*SAFT results presented in this section highlight the capabilities of the theory to correctly capture hydrogen bonding/association interactions in polyatomic systems. Even the fundamental case of associating homopolymers considered in this section challenges the theory to capture the presence and absence of mesophases and liquid−liquid phase behavior, as well as intriguing reappearing phases in the phase diagram. More detailed extensions of this study can be conducted, specifically to study and understand more complex, self-assembling associating polymer systems in the bulk. Such work includes multicomponent (ternary and higher) polymer blends, asymmetric cases (unequal concentrations and/or unequal chain lengths of the polymers), and multiple bonding sites on multiple polymer segments of varying size (leading to other supramolecular architectures beyond the diblock copolymer considered in this work). As the architecture becomes more complicated, the self-assembly of more complex, hierarchical morphologies can arise (for example, the self-assembly of Archimedean tiling patterns[3−5,7]). Future studies of *i*SAFT to such challenging problems could aid in the development and production of high performance soft materials and separation applications.

IV. Conclusions

The *i*SAFT density functional theory has been extended to associating polyatomic molecular systems, using the inhomogeneous form of the association functional. The approach provides a very accurate method for modeling a wide range of complex associating polyatomic systems, capable of investigating the full range of association for any bonding scheme. In this work, the ability of the theory to model associating polymers near surfaces and in the bulk over a wide range of conditions was demonstrated. Even for the fundamental associating polymers chosen in this work, the results highlight a wide range of complex behaviors, demonstrating how reversible bonding governs the structure of a fluid near a surface (in good agreement with available simulation data), the molecular connectivity (formation of supramolecules and complex architectures), and the phase behavior of the system (including reentrant order−disorder phase transitions). The introduction of hydrogen bonding interactions thus leads to a new class of self-assembling, highly functional materials. It is evident that *i*SAFT could significantly aid in the understanding and experimental design of more complex, associating polymer systems, with applications to the fields of biomolecules, separations, high performance soft materials, polymer mediated adhesion and lubrication, and polymer−inorganic nanocomposites.

Acknowledgment. The financial support for this work was provided by the Robert A. Welch Foundation (Grant No. C1241) and by the National Science Foundation (CBET-0756166). This work was supported in part by the Shared University Grid at Rice funded by NSF under grant EIA-0216467, and a partnership between Rice University, Sun Microsystems, and Sigma Solutions, Inc.

Supporting Information Available: Detailed expressions and derivations for the association terms presented in this paper. This material is available free of charge via the Internet at http://pubs.acs.org.

References and Notes

(1) Li, J.; Li, X.; Ni, X. P.; Wang, X.; Li, H. Z.; Leong, K. W. *Biomaterials* **2006**, *27*, 4132–4140.
(2) Sijbesma, R. P.; Beijer, F. H.; Brunsveld, L.; Folmer, B. J. B.; Hirschberg, J.; Lange, R. F. M.; Lowe, J. K. L.; Meijer, E. W. *Science* **1997**, *278*, 1601–1604.
(3) Asari, T.; Arai, S.; Takano, A.; Matsushita, Y. *Macromolecules* **2006**, *39*, 2232–2237.
(4) Asari, T.; Matsuo, S.; Takano, A.; Matsushita, Y. *Macromolecules* **2005**, *38*, 8811–8815.
(5) Asari, T.; Matsuo, S.; Takano, A.; Matsushita, Y. *Polym. J.* **2006**, *38*, 258–263.
(6) Beck, J. B.; Rowan, S. J. *J. Am. Chem. Soc.* **2003**, *125*, 13922–13923.
(7) Matsushita, Y. *Macromolecules* **2007**, *40*, 771–776.
(8) Noro, A.; Matsushita, Y.; Lodge, T. P. *Macromolecules* **2008**, *41*, 5839–5844.
(9) Ruokolainen, J.; Makinen, R.; Torkkeli, M.; Makela, T.; Serimaa, R.; ten Brinke, G.; Ikkala, O. *Science* **1998**, *280*, 557–560.
(10) Ruokolainen, J.; Saariaho, M.; Ikkala, O.; ten Brinke, G.; Thomas, E. L.; Torkkeli, M.; Serimaa, R. *Macromolecules* **1999**, *32*, 1152–1158.
(11) Shen, J. G.; Hogen-Esch, T. *J. Am. Chem. Soc.* **2008**, *130*, 10866.
(12) Dai, J.; Goh, S. H.; Lee, S. Y.; Siow, K. S. *Polym. J.* **1994**, *26*, 905–911.
(13) Pan, J.; Chen, M. F.; Warner, W.; He, M. Q.; Dalton, L.; Hogen-Esch, T. E. *Macromolecules* **2000**, *33*, 7835–7841.
(14) Xiang, M. L.; Jiang, M.; Zhang, Y. B.; Wu, C.; Feng, L. X. *Macromolecules* **1997**, *30*, 2313–2319.
(15) Dai, L. M.; Toprakcioglu, C. *Macromolecules* **1992**, *25*, 6000–6006.
(16) Kim, H. S.; Lau, W.; Kumacheva, E. *Macromolecules* **2000**, *33*, 4561–4567.
(17) Kim, S. D.; Torkelson, J. M. *Macromolecules* **2002**, *35*, 5943–5952.
(18) Ruths, M.; Granick, S. *J. Phys. Chem. B* **1999**, *103*, 8711–8721.
(19) Tanaka, F.; Ishida, M. *Macromolecules* **1997**, *30*, 1836–1844.
(20) Tanaka, F.; Ishida, M.; Matsuyama, A. *Macromolecules* **1991**, *24*, 5582–5589.
(21) Angerman, H. J.; ten Brinke, G. *Macromolecules* **1999**, *32*, 6813–6820.
(22) Dormidontova, E.; ten Brinke, G. *Macromolecules* **1998**, *31*, 2649–2660.
(23) Feng, E. H.; Lee, W. B.; Fredrickson, G. H. *Macromolecules* **2007**, *40*, 693–702.
(24) Lee, W. B.; Elliott, R.; Katsov, K.; Fredrickson, G. H. *Macromolecules* **2007**, *40*, 8445–8454.
(25) Geisinger, T.; Muller, M.; Binder, K. *J. Chem. Phys.* **1999**, *111*, 5241–5250.
(26) Geisinger, T.; Muller, M.; Binder, K. *J. Chem. Phys.* **1999**, *111*, 5251–5258.
(27) Ayyagari, C.; Bedrov, D.; Smith, G. D. *Polymer* **2004**, *45*, 4549–4558.
(28) Guo, L.; Luijten, E. *J. Polym. Sci., Part B: Polym. Phys.* **2005**, *43*, 959–969.
(29) Huh, J.; Ikkala, O.; tenBrinke, G. *Macromolecules* **1997**, *30*, 1828–1835.
(30) Huh, J.; ten Brinke, G. *J. Chem. Phys.* **1998**, *109*, 789–797.
(31) Koga, T.; Tanaka, F. *Eur. Phys. J. E* **2005**, *17*, 115–118.
(32) Sung, B. J.; Yethiraj, A. *J. Chem. Phys.* **2003**, *119*, 6916–6924.
(33) Chen, C. C.; Dormidontova, E. E. *Macromolecules* **2006**, *39*, 9528–9538.
(34) Malvaldi, M.; Allegra, G.; Ciardelli, F.; Raos, G. *J. Phys. Chem. B* **2005**, *109*, 18117–18126.
(35) Malvaldi, M.; Bruzzone, S.; Raos, G.; Allegra, G. *J. Phys. Chem. B* **2007**, *111*, 4141–4149.
(36) Wu, J. Z. *AIChE J.* **2006**, *52*, 1169–1193.
(37) Chapman, W. G. Ph.D. Thesis, Cornell University, 1988.
(38) Wertheim, M. S. *J. Stat. Phys.* **1984**, *35*, 19.
(39) Wertheim, M. S. *J. Stat. Phys.* **1984**, *35*, 35.
(40) Wertheim, M. S. *J. Stat. Phys.* **1986**, *42*, 459.
(41) Wertheim, M. S. *J. Stat. Phys.* **1986**, *42*, 477.
(42) Segura, C. J.; Chapman, W. G.; Shukla, K. P. *Mol. Phys.* **1997**, *90*, 759–771.
(43) Patrykiejew, A.; Sokolowski, S.; Henderson, D. *Mol. Phys.* **1998**, *95*, 211–218.

(44) Pizio, O.; Patrykiejew, A.; Sokolowski, S. *J. Chem. Phys.* **2000**, *113*, 10761–10767.
(45) Segura, C. J.; Vakarin, E. V.; Chapman, W. G.; Holovko, M. F. *J. Chem. Phys.* **1998**, *108*, 4837–4848.
(46) Segura, C. J.; Zhang, J.; Chapman, W. G. *Mol. Phys.* **2001**, *99*, 1–12.
(47) Tripathi, S.; Chapman, W. G. *J. Chem. Phys.* **2003**, *118*, 7993–8003.
(48) Yu, Y. X.; Wu, J. Z. *J. Chem. Phys.* **2002**, *116*, 7094–7103.
(49) Bryk, P.; Sokolowski, S.; Pizio, O. *J. Chem. Phys.* **2006**, *125*, 024909.
(50) Fu, D.; Wu, J. Z. *Ind. Eng. Chem. Res.* **2005**, *44*, 1120–1128.
(51) Gloor, G. J.; Jackson, G.; Blas, F. J.; del Rio, E. M.; de Miguel, E. *J. Phys. Chem. C* **2007**, *111*, 15513–15522.
(52) Gloor, G. J.; Jackson, G.; Blas, F. J.; del Rio, E. M.; de Miguel, E. *J. Chem. Phys.* **2004**, *121*, 12740–12759.
(53) Bucior, K.; Fischer, J.; Patrykiejew, A.; Tscheliessnig, R.; Sokolowski, S. *J. Chem. Phys.* **2007**, *126*, 094704.
(54) Jain, S.; Dominik, A.; Chapman, W. G. *J. Chem. Phys.* **2007**, *127*, 244904.
(55) Tripathi, S.; Chapman, W. G. *Phys. Rev. Lett.* **2005**, *94*, 087801.
(56) Tripathi, S.; Chapman, W. G. *J. Chem. Phys.* **2005**, *122*, 094506.
(57) Dominik, A.; Tripathi, S.; Chapman, W. G. *Ind. Eng. Chem. Res.* **2006**, *45*, 6785–6792.
(58) Jain, S.; Chapman, W. G. *Mol. Phys.* **2009**, *107*, 1–17.
(59) Jain, S.; Jog, P.; Weinhold, J.; Srivastava, R.; Chapman, W. G. *J. Chem. Phys.* **2008**, *128*, 154910.
(60) Bymaster, A.; Jain, S.; Chapman, W. G. *J. Chem. Phys.* **2008**, *128*, 13.
(61) Bymaster, A. S. Ph.D. Thesis, Rice University, 2009.
(62) Jain, S. Ph.D. Thesis, Rice University, 2009.
(63) Chandler, D.; Weeks, J. D. *Phys. Rev. Lett.* **1970**, *25*, 149.
(64) Weeks, J. D.; Chandler, D.; Andersen, H. C. *J. Chem. Phys.* **1971**, *54*, 5237.
(65) Evans, R. In *Fundamentals of Inhomogeneous Fluids*; Henderson, D., Ed.; Marcel-Dekker: New York, 1992; pp 85−175.
(66) Rosenfeld, Y. *Phys. Rev. A* **1990**, *42*, 5978–5989.
(67) Rosenfeld, Y. *Phys. Rev. Lett.* **1989**, *63*, 980–983.
(68) McQuarrie, D. A. *Statistical Mechanics*; Unversity Science Books: Sausalito, CA, 2000.
(69) Tang, Y. P.; Wu, J. Z. *Phys. Rev. E* **2004**, *70*.
(70) Muller, M.; MacDowell, L. G.; Yethiraj, A. *J. Chem. Phys.* **2003**, *118*, 2929.
(71) Reddy, G.; Yethiraj, A. *J. Chem. Phys.* **2004**, *121*, 4203.
(72) Toxvaerd, S. *J. Chem. Phys.* **1976**, *64*, 2863.
(73) Carnahan, N. F.; Starling, K. E. *J. Chem. Phys.* **1969**, *51*, 635.
(74) Yethiraj, A.; Hall, C. K. *J. Chem. Phys.* **1991**, *94*, 3943–3948.
(75) Tarazona, P. *Phys. Rev. A* **1985**, *31*, 2672.
(76) Tarazona, P. *Phys. Rev. A* **1985**, *32*, 3148.
(77) Malijevsky, A.; Bryk, P.; Sokolowski, S. *Phys. Rev. E* **2005**, *72*, 032801.
(78) Yu, Y.-X.; Wu, J. *J. Chem. Phys.* **2002**, *117*, 2368.
(79) Frischknecht, A. L.; Curro, J. G.; Frink, L. J. D. *J. Chem. Phys.* **2002**, *117*, 10398–10411.
(80) Walker, J. S.; Vause, C. A. *Sci. Am.* **1987**, *256*, 98.

JP102677M